On the feasibility of situational awareness in millimeter wave massive MIMO systems

On the Feasibility of Situational Awareness in Millimeter Wave Massive MIMO Systems

Rico Mendrzik,† Henk Wymeersch,* and Gerhard Bauch,†
†Institute of Communications, Hamburg University of Technology
* Department of Electrical Engineering, Chalmers University of Technology
Email: {mendrzik, bauch}@tuhh.de, henkw@chalmers.se

***Abstract*—Situational awareness in wireless networks refers to the availability of information on the states of mobile devices and their propagation environments. Recent studies have shown that the position, orientation, and clock offset of a mobile device can be estimated jointly with a map of reflecting or scattering features in the propagation environment based on the link to a single base station. Yet, it is unknown how important system parameters such as the bandwidth, the number of antennas, and the signal-to-noise ratio affect the estimation accuracy and hence the feasibility of situational awareness. We address this open question by studying the Cramér-Rao lower bound of the joint estimation problem. Particularly, we provide an analytical expression for the corresponding Fisher information matrix and inspect the Cramér-Rao lower bound via numerical simulations. Our results reveal the following insights. First, the reflection loss of objects in the propagation environment has a profound impact on the estimation accuracy of the states of mobile devices and their maps. Second, the massiveness of arrays is a key enabler for accurate state and map estimation and finally, the geometry of the scenario affects the estimation accuracy profoundly.**

I. Introduction

New physical (PHY) layers in fifth generation (5G) systems and beyond will include millimeter wave (mmWave) massive multiple-input multiple-output (mMIMO) technology [1]. The combination of wide bandwidth in the mmWave frequency bands and large number of antennas of mMIMO arrays has the potential to revolutionize communication-based positioning. Beyond positioning, systems that employ mmWave mMIMO technology enable the estimation of other user equipment (UE) states such as orientation and clock offset. Furthermore, such systems make it possible to determine the positions of reflectors and scatterers, resulting in a simultaneous mapping of the propagation environment [2]–[6]. These capabilities are unprecedented in the history of communication systems and the availability of such information will enable situational awareness in future wireless networks, i.e. geometric information on the base station, the UE states, and the propagation environment will become available and can be harnessed to assist and improve communications [2], [7].

Recent theoretical studies [8]–[10] already provided insights into the localization capabilities of mmWave mMIMO systems. In [8] it was shown that it is possible to localize UEs with a single base station and [9] investigated the impact of the transmission mode (uplink or downlink) on the positioning accuracy. Another important finding was presented in [10], where it was analytically shown that multipath components increase the localization accuracy. [8]–[10] assume that the base station and UE are perfectly synchronized.

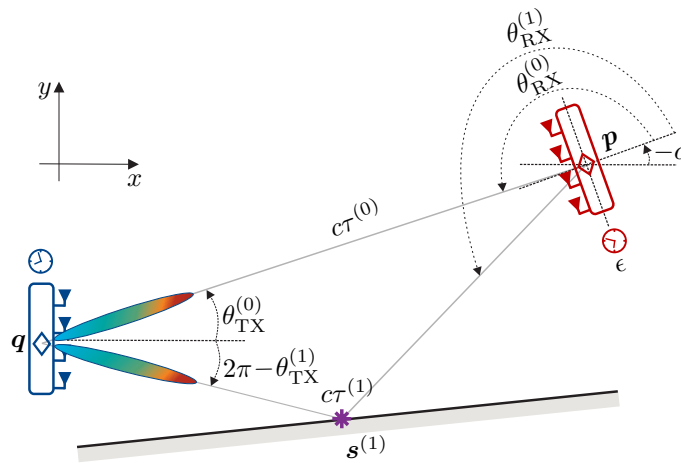

Fig. 1. Joint parameter estimation problem in 5G mmWave mMIMO systems. The goal is to infer the position $\boldsymbol{p}$, orientation α, clock offset ϵ, and points of incidence $\boldsymbol{s}_j, j = 1, 2, \cdots, N_{\mathrm{P}}$ based on the noisy channel measurements (AOAs $\hat{\theta}_{\mathrm{RX}}^{(j)}$, AODs $\hat{\theta}_{\mathrm{TX}}^{(j)}$, and delays $\hat{\tau}^{(j)}, j = 0, 1, \cdots, N_{\mathrm{P}}$) that can be deduced from the received signal.

In this article we present the closed-form solution of the Fisher information matrix (FIM) of the joint position, clock offset, orientation, and map estimation problem in mmWave mMIMO systems. We study the corresponding Cramér-Rao lower bound (CRLB) numerically and present novel insights regarding the feasibility of situational awareness. Our analyses advance the understanding of joint positioning, synchronization, orientation estimation, and mapping by revealing the following:

- Antenna-array scaling provides larger gains than bandwidth scaling in terms of the estimation accuracy.
- High reflection losses incurred on non-line-of-sight (NLOS) paths can render synchronization and hence situational awareness infeasible.

Notation: Random variables are displayed in sans serif, upright fonts; their realizations in serif, italic fonts. Vectors and matrices are denoted by bold lowercase and uppercase letters, respectively. For example, a random variable and its realization are denoted by x and x; a random vector and its realization are denoted by $\mathbf{x}$ and $\boldsymbol{x}$. An estimate of a parameter is denoted with the superscript hat, e.g. $\hat{x}$. Furthermore, $\|\boldsymbol{x}\|$, $\boldsymbol{x}^{\mathrm{T}}$, $\boldsymbol{x}^{\mathrm{H}}$ denote the Euclidean norm, the transpose, and transpose conjugate-complex of vector $\boldsymbol{x}$, respectively.

II. System Model and Problem Formulation

We provide a description of our system model by depicting the geometry and elaborating on communication chain.

A. Geometric Constellation

An exemplary scenario of the geometry is depicted in Fig. 1. A fixed base station with known but arbitrary position[1] $\boldsymbol{q}=[q_{\mathrm{x}}\ q_{\mathrm{y}}]^{\mathrm{T}}$ is considered. The base station is serving a mobile UE which is located at $\boldsymbol{p}=[p_{\mathrm{x}}\ p_{\mathrm{y}}]^{\mathrm{T}}$. The propagation environment consists of specular reflection points and scattering points. We use the term *point of incidence* to summarize both specular reflection points and scattering points. The total number of incidence points is L and their positions are denoted by $\boldsymbol{s}^{(j)}=[s_{\mathrm{x}}^{(j)}\ s_{\mathrm{y}}^{(j)}]^{\mathrm{T}}, j=1,2,\cdots,N_{\mathrm{P}}$. We assume that the UE position and the points of incidence are static for the duration of a transmission burst.

B. Transmitter and Receiver Models

We consider downlink transmission from the base station to the UE, i.e. the base station is the transmitter (TX) and the UE is the receiver (RX). The base station is equipped with an array with N_{TX} antennas. The geometry of the array is arbitrary but known and its array response vector is given by

$$\boldsymbol{a}_{\mathrm{TX}}(\theta_{\mathrm{TX}})=\frac{1}{\sqrt{N_{\mathrm{TX}}}}\exp(-i\boldsymbol{\Delta}_{\mathrm{TX}}^{\mathrm{T}}\boldsymbol{k}(\theta_{\mathrm{TX}})), \tag{1}$$

where $i=\sqrt{-1}$, θ_{TX} is the incidence angle, $\boldsymbol{k}(\theta_{\mathrm{TX}})=2\pi/\lambda[\cos(\theta_{\mathrm{TX}})\ \sin(\theta_{\mathrm{TX}})]^{\mathrm{T}}$ is the wave vector, in which λ denotes the wavelength. $\boldsymbol{\Delta}_{\mathrm{TX}}\in\mathbb{R}^{2\times N_{\mathrm{TX}}}$ is a matrix that contains the positions of the antenna elements in its columns, i.e. $\boldsymbol{\Delta}_{\mathrm{TX}}=[\mathbf{u}_{\mathrm{TX},1}\ \mathbf{u}_{\mathrm{TX},2}\cdots\mathbf{u}_{\mathrm{TX},N_{\mathrm{TX}}}]^{\mathrm{T}}$ and $\mathbf{u}_{\mathrm{TX},m}$ is the position of the mth element of the transmitter array. The orientation of the transmitter array is denoted by ϕ. All angles are measured counter-clockwise with respect to the positive x-axis of the reference frame. Without loss of generality, we consider $\phi=0$.

The receiver is also equipped with an antenna array of arbitrary but known geometry. This array consists of N_{RX} antennas. The orientation of the array with respect to the global reference frame is denoted by α (see Fig. 1). The array response vector of the receiver can be obtained by considering (1) and modifying the subscripts.

C. Signal and Channel Models

We consider the transmission of orthogonal frequency division multiplexing (OFDM) signals which are modulated on a mmWave carrier with frequency f_{c} as envisioned for 5G systems. The transmitted signal contains N_{SC} subcarriers that are symmetrically spaced around the carrier frequency f_{c}. Hence the total bandwidth of $B=N_{\mathrm{SC}}\Delta f$, where $\Delta f=1/T_{\mathrm{s}}$ denotes the subcarrier spacing and T_{s} is the symbol duration. The base station transmits N_{B} beams[2] $\boldsymbol{f}_i$, i.e. $\boldsymbol{F}=[\boldsymbol{f}_1\ \boldsymbol{f}_2\cdots\boldsymbol{f}_{N_{\mathrm{B}}}]\in\mathbb{C}^{N_{\mathrm{TX}}\times N_{\mathrm{B}}}$. The symbols $x_{i,n}$ transmitted on the nth subcarrier are known pilot symbols from an arbitrary complex-valued modulation alphabet with $\mathbb{E}(|x_{i,n}|^2)=1$. They are denoted by $\boldsymbol{x}_n=[x_{1,n}\ x_{2,n}\cdots x_{N_{\mathrm{B}},n}]^{\mathrm{T}}\in\mathbb{C}^{N_{\mathrm{B}}}$. The complex-valued baseband signal is generated via an N_{SC}-point inverse discrete Fourier transform (IDFT). A cyclic prefix (CP) of length T_{CP} is added and we assume that the duration of the CP exceeds the delay spread of the channel. In summary, the baseband signal of the nth subcarrier can be expressed as

$$\tilde{\boldsymbol{x}}_n=\sqrt{\frac{E_{\mathrm{S}}}{N_{\mathrm{B}}N_{\mathrm{SC}}}}\boldsymbol{F}\boldsymbol{x}_n, \tag{2}$$

where E_{S} is the energy per MIMO-OFDM symbol.

The signal is transmitted over a sparse mmWave mMIMO channel with $N_{\mathrm{P}}+1$ paths whose transformation matrix in the equivalent baseband is given by [11]

$$\boldsymbol{H}_n=\sum_{j=0}^{N_{\mathrm{P}}}\underbrace{\exp\left(-\frac{i2\pi n\tau^{(j)}}{NT_s}\right)\frac{h^{(j)}}{\sqrt{\gamma^{(j)}\rho^{(j)}}}}_{\triangleq\xi_n^{(j)}}\boldsymbol{a}_{\mathrm{RX}}(\theta_{\mathrm{RX}}^{(j)})\boldsymbol{a}_{\mathrm{TX}}^{\mathrm{H}}(\theta_{\mathrm{TX}}^{(j)}) \tag{3}$$

where $h^{(j)}$, $\gamma^{(j)}$, $\rho^{(j)}$, $\tau^{(j)}$, $\theta_{\mathrm{TX}}^{(j)}$, $\theta_{\mathrm{RX}}^{(j)}$ denote the complex-valued channel coefficient, path loss, reflection loss, delay, AOD, and AOA of the jth path, respectively. Without loss of generality, we assume that the index $j=0$ refers to the line-of-sight (LOS) path and $j>0$ are NLOS paths. Obviously, the LOS path does not incur a reflection loss, i.e. $\rho^{(0)}=1$. Note that (3) assumes a narrow-band array model, meaning that $f_{\mathrm{c}}+n\Delta f\approx f_{\mathrm{c}}$ for all subcarriers n.

The received signal on the nth subcarrier after CP removal and discrete Fourier transform (DFT) is given by

$$\mathbf{r}_n=\underbrace{\sqrt{\frac{E_{\mathrm{S}}}{N_{\mathrm{B}}N_{\mathrm{SC}}}}\boldsymbol{H}_n\boldsymbol{F}}_{\triangleq\boldsymbol{\mu}_n}\boldsymbol{x}_n+\mathbf{n}_n, \tag{4}$$

in which $\boldsymbol{\mu}_n$ is the noise-free (average) observation on subcarrier n and $\mathbf{n}_n=[\mathsf{n}_{1,n}\ \cdots\ \mathsf{n}_{2,n}\ \mathsf{n}_{N_{\mathrm{RX}},n}]^{\mathrm{T}}$ is a vector of statistically independent complex-valued zero-mean additive white Gaussian noise (AWGN) terms $\mathsf{n}_{m,n}, m=1,2,\cdots,N_{\mathrm{RX}}$ with power spectral density $N_0/2$ per real dimension . We use the following definition of the signal to noise power ratio (SNR): $\mathrm{SNR}\triangleq\mathbb{E}\{\boldsymbol{\mu}_n^{\mathrm{H}}\boldsymbol{\mu}_n/(\mathbf{n}_n^{\mathrm{H}}\mathbf{n}_n)\}$.

Remark: It is worth mentioning that we assume that the beamformers $\boldsymbol{f}_b, b=1,2,\cdots,N_{\mathrm{B}}$ are known to the UE. This knowledge is a prerequisite for AOD estimation. Moreover, we assume that the base station and UE are synchronized with a temporal accuracy sufficing communications, i.e. the local clock of the UE is aligned with the global clock of the base station, up to fractions of the symbol duration. However, a residual clock offset ϵ exists which needs to be estimated to obtain precise path delays and hence allow for accurate ranging.

D. Parameter Spaces

We consider two different parameter spaces that are tightly coupled with each other: (i) channel parameters and (ii) position-related parameters. Channel parameters are the delays $\tau^{(j)}$, AODs $\theta_{\mathrm{TX}}^{(j)}$, AOAs $\theta_{\mathrm{RX}}^{(j)}$, and complex channel gains $h^{(j)}$ of all channel paths $j=0,1,\cdots N_{\mathrm{P}}$. In the parlance of this article, the position $\boldsymbol{p}$, orientation α, clock offset ϵ, and points of incidence $\boldsymbol{s}^{(j)}, j=1,2,\cdots N_{\mathrm{P}}$ are position-related

[1] We consider a two-dimensional (2D) system model for the simplicity of the analysis. Extending our model to three-dimensional (3D) space is straightforward.

[2] Our analysis considers fully digital beamforming to study the CRLB. Since constraints on the choice of the beams $\boldsymbol{f}_i, \forall i$ due to hybrid analog-digital transceiver/receiver architectures will only reduce the estimation accuracy, our analysis investigates the fundamental limits.

parameters. The mathematical relationship between channel parameters and position-related parameters is summarized in the following:

$$\tau^{(0)}(\boldsymbol{p},\epsilon) = \frac{||\boldsymbol{q}-\boldsymbol{p}||}{c} + \epsilon, \tag{5a}$$

$$\tau^{(j)}(\boldsymbol{p},\epsilon,\boldsymbol{s}^{(j)}) = \frac{||\boldsymbol{q}-\boldsymbol{s}^{(j)}|| + ||\boldsymbol{s}^{(j)}-\boldsymbol{p}||}{c} + \epsilon, \tag{5b}$$

$$\theta_{\mathrm{TX}}^{(0)}(\boldsymbol{p}) = \operatorname{atan2}\left(p_{\mathrm{y}}-q_{\mathrm{y}}, p_{\mathrm{x}}-q_{\mathrm{x}}\right), \tag{5c}$$

$$\theta_{\mathrm{TX}}^{(j)}(\boldsymbol{s}^{(j)}) = \operatorname{atan2}\left(s_{\mathrm{y}}^{(j)}-q_{\mathrm{y}}, s_{\mathrm{x}}^{(j)}-q_{\mathrm{x}}\right), \tag{5d}$$

$$\theta_{\mathrm{RX}}^{(0)}(\boldsymbol{p},\alpha) = \operatorname{atan2}\left(q_{\mathrm{y}}-p_{\mathrm{y}}, q_{\mathrm{x}}-p_{\mathrm{x}}\right) - \alpha, \tag{5e}$$

$$\theta_{\mathrm{RX}}^{(j)}(\boldsymbol{p},\alpha,\boldsymbol{s}^{(j)}) = \operatorname{atan2}\left(s_{\mathrm{y}}^{(j)}-p_{\mathrm{y}}, s_{\mathrm{x}}^{(j)}-p_{\mathrm{x}}\right) - \alpha, \tag{5f}$$

where $\operatorname{atan2}(\cdot)$ is the four-quadrant inverse tangent. For notational convenience, we summarize all channel parameters in the vector $\tilde{\boldsymbol{\eta}}$ whose entries are given by

$$\tilde{\boldsymbol{\eta}} \triangleq [\boldsymbol{\tau}^{\mathrm{T}}\ \boldsymbol{\theta}_{\mathrm{TX}}^{\mathrm{T}}\ \boldsymbol{\theta}_{\mathrm{RX}}^{\mathrm{T}}\ \boldsymbol{h}_{\mathrm{I}}^{\mathrm{T}}\ \boldsymbol{h}_{\mathrm{Q}}^{\mathrm{T}}]^{\mathrm{T}},$$

in which the delays $\boldsymbol{\tau} = [\tau^{(0)}\ \tau^{(1)} \cdots \tau^{(N_{\mathrm{P}})}]^{\mathrm{T}}$, AODs $\boldsymbol{\theta}_{\mathrm{TX}} = [\theta_{\mathrm{TX}}^{(0)}\ \theta_{\mathrm{TX}}^{(1)} \cdots \theta_{\mathrm{TX}}^{(N_{\mathrm{P}})}]^{\mathrm{T}}$, AOAs $\boldsymbol{\theta}_{\mathrm{RX}} = [\theta_{\mathrm{RX}}^{(0)}\ \theta_{\mathrm{RX}}^{(1)} \cdots \theta_{\mathrm{RX}}^{(N_{\mathrm{P}})}]^{\mathrm{T}}$, and the channel gains $\boldsymbol{h}_{\mathrm{I}} = [h_{\mathrm{I}}^{(0)}\ h_{\mathrm{I}}^{(1)} \cdots h_{\mathrm{I}}^{(N_{\mathrm{P}})}]^{\mathrm{T}}$ and $\boldsymbol{h}_{\mathrm{Q}} = [h_{\mathrm{Q}}^{(0)}\ h_{\mathrm{Q}}^{(1)} \cdots h_{\mathrm{Q}}^{(N_{\mathrm{P}})}]^{\mathrm{T}}$ are grouped. Moreover, we define the position-related parameter vector $\boldsymbol{\eta}$ as

$$\boldsymbol{\eta} \triangleq [\boldsymbol{p}^{\mathrm{T}}\ \alpha\ \epsilon\ \boldsymbol{s}^{(1)\mathrm{T}}\ \boldsymbol{s}^{(2)\mathrm{T}} \cdots \boldsymbol{s}^{(N_{\mathrm{P}})\mathrm{T}}]^{\mathrm{T}}.$$

Our principle question in this study is to understand the conditions which render situational awareness feasible, i.e. in which scenarios can we obtain position $\boldsymbol{p}$, orientation α, clock offset ϵ, and map $\boldsymbol{s}^{(j)}, \forall j$ estimates with reasonable accuracy? To answer this question, we first note – as may be obvious to the expert reader – that the problem at hand is a nonlinear estimation problem under additive noise and we may instead ask: What is the smallest possible mean squared error (MSE) that an estimator can provide under specified conditions? The latter question can be addressed via the concept of Fisher information and the CRLB, as will be outlined in the next section.

III. Fisher Information Matrices and Error Bounds

We shall use the concept of Fisher information to study the properties of the estimation problem. First, we will briefly review the notion of Fisher information and equivalent Fisher information. We will use both concepts to derive an analytical expression of the FIM $\boldsymbol{J}_{\boldsymbol{\eta}}$ of the position-related parameters. In the pursuit of deriving this FIM, we first develop the FIM $\boldsymbol{J}_{\tilde{\boldsymbol{\eta}}}$ of the channel parameters and subsequently, we apply the concept of equivalent Fisher information to obtain the equivalent Fisher information matrix (EFIM) $\boldsymbol{J}_{\tilde{\boldsymbol{\eta}}_1}^{\mathrm{e}}$ of the relevant channel parameters (delays, AODs, and AOAs) that are functions of the position related-parameters; see (5). Finally, we obtain the FIM $\boldsymbol{J}_{\boldsymbol{\eta}}$ of the position-related parameters (position $\boldsymbol{p}$, orientation α, clock offset ϵ, and points of incidence $\boldsymbol{s}^{(N_{\mathrm{P}})}, j = 1, 2, \cdots, N_{\mathrm{P}}$) by applying a Jacobian transformation to the EFIM $\boldsymbol{J}_{\tilde{\boldsymbol{\eta}}_1}^{\mathrm{e}}$. We conclude this section by defining the error bounds for the position-related parameters.

A. Fundamentals and Definitions

1) Information Inequality: Let $\hat{\boldsymbol{\eta}}$ be an unbiased estimator of parameter $\boldsymbol{\eta}$ based on the observation vector $\boldsymbol{r}$. Then, the MSE matrix of $\hat{\boldsymbol{\eta}}$ satisfies the information inequality [12]–[14]

$$\mathbb{E}_{\mathbf{r}}\left[(\hat{\boldsymbol{\eta}}-\boldsymbol{\eta})(\hat{\boldsymbol{\eta}}-\boldsymbol{\eta})^{\mathrm{T}}\right] \succcurlyeq \boldsymbol{J}_{\boldsymbol{\eta}}^{-1}, \tag{6}$$

where $\boldsymbol{J}_{\boldsymbol{\eta}}$ is the FIM of $\boldsymbol{\eta}$, given by

$$\boldsymbol{J}_{\boldsymbol{\eta}} = \mathbb{E}_{\mathbf{r}}\left[-\frac{\partial^2}{\partial\boldsymbol{\eta}\partial\boldsymbol{\eta}^{\mathrm{T}}}\ln f(\boldsymbol{r}|\boldsymbol{\eta})\right], \tag{7}$$

in which $f(\boldsymbol{r}|\boldsymbol{\eta})$ is the likelihood function of the observation $\mathbf{r}$ conditioned on the parameter vector $\boldsymbol{\eta}$.

2) Equivalent Fisher Information: Given a parameter vector $\boldsymbol{\eta} \triangleq [\boldsymbol{\eta}_1^{\mathrm{T}}\ \boldsymbol{\eta}_2^{\mathrm{T}}]^{\mathrm{T}}$ with corresponding FIM

$$\boldsymbol{J}_{\boldsymbol{\eta}} \triangleq \begin{bmatrix} \boldsymbol{J}_{\boldsymbol{\eta}_1\boldsymbol{\eta}_1} & \boldsymbol{J}_{\boldsymbol{\eta}_1\boldsymbol{\eta}_2} \\ \boldsymbol{J}_{\boldsymbol{\eta}_1\boldsymbol{\eta}_2}^{\mathrm{T}} & \boldsymbol{J}_{\boldsymbol{\eta}_2\boldsymbol{\eta}_2} \end{bmatrix}, \tag{8}$$

the EFIM of $\boldsymbol{\eta}_1$ is obtained by [15]

$$\boldsymbol{J}_{\boldsymbol{\eta}_1}^{\mathrm{e}} \triangleq \boldsymbol{J}_{\boldsymbol{\eta}_1\boldsymbol{\eta}_1} - \boldsymbol{J}_{\boldsymbol{\eta}_1\boldsymbol{\eta}_2}\boldsymbol{J}_{\boldsymbol{\eta}_2\boldsymbol{\eta}_2}^{-1}\boldsymbol{J}_{\boldsymbol{\eta}_1\boldsymbol{\eta}_2}^{\mathrm{T}}. \tag{9}$$

Intuitively, the fact that the parameters of $\boldsymbol{\eta_2}$ are not perfectly known, leads to a loss in information. This loss is quantified by $\boldsymbol{J}_{\boldsymbol{\eta}_1\boldsymbol{\eta}_2}\boldsymbol{J}_{\boldsymbol{\eta}_2\boldsymbol{\eta}_2}^{-1}\boldsymbol{J}_{\boldsymbol{\eta}_1\boldsymbol{\eta}_2}^{\mathrm{T}}$.

B. Channel Fisher Information Matrix

The general definition of the FIM matrix is given in (7). However, the properties of the channel parameter estimation problem allow for some simplifications of the expression in (7). In case of N_{SC} independent complex-valued observations $\mathbf{r}_n, n = 1, 2, \cdots N_{\mathrm{SC}}$ obtained on orthogonal subcarriers, the entry in the kth row and l^{th} column of the channel FIM can be written as

$$[\boldsymbol{J}_{\tilde{\boldsymbol{\eta}}}]_{k,l} \triangleq \sum_{n=1}^{N_s} \frac{2}{N_0}\mathcal{R}\left\{\frac{\partial\boldsymbol{\mu}_n^{\mathrm{H}}}{\partial[\tilde{\boldsymbol{\eta}}]_k}\frac{\partial\boldsymbol{\mu}_n}{\partial[\tilde{\boldsymbol{\eta}}]_l}\right\}, \tag{10}$$

where $\mathcal{R}\{\cdot\}$ is the real-part operator. Recall that $\boldsymbol{\mu}_n$ is a function of the channel parameters $\tilde{\boldsymbol{\eta}}$ (though not explicitly shown). Considering (10), we observe that the channel FIM $\boldsymbol{J}_{\tilde{\boldsymbol{\eta}}}$ is readily obtained from the partial derivatives $\partial\boldsymbol{\mu}_n^{\mathrm{H}}/\partial[\tilde{\boldsymbol{\eta}}]_l, \forall l$ of the noise-free observation in (4). For convenience of the reader, we summarize these partial derivatives in Appendix A.

C. Equivalent Channel Fisher Information Matrix

We like to stress that neither the inphase $\boldsymbol{h}_{\mathrm{I}}$ nor the quadrature $\boldsymbol{h}_{\mathrm{Q}}$ components affect the position-related parameters directly. However, the uncertainty regarding these parameters decreases the Fisher information of the other channel parameters (delays, AODs, and AOAs). Hence the complex channel gains have an indirect impact on the position-related parameters. We can account for this fact by considering the concept of equivalent Fisher information as presented in section III-A2. Introducing the reduced-size channel parameter vectors $\tilde{\boldsymbol{\eta}}_1 \triangleq [\boldsymbol{\tau}^{\mathrm{T}}\ \boldsymbol{\theta}_{\mathrm{TX}}^{\mathrm{T}}\ \boldsymbol{\theta}_{\mathrm{RX}}^{\mathrm{T}}]^{\mathrm{T}}$ and $\tilde{\boldsymbol{\eta}}_2 \triangleq [\boldsymbol{h}_{\mathrm{I}}^{\mathrm{T}}\ \boldsymbol{h}_{\mathrm{Q}}^{\mathrm{T}}]^{\mathrm{T}}$, we follow (9) and obtain the EFIM of $\tilde{\boldsymbol{\eta}}_1$ via

$$\boldsymbol{J}_{\tilde{\boldsymbol{\eta}}_1}^{\mathrm{e}} = \boldsymbol{J}_{\tilde{\boldsymbol{\eta}}_1\tilde{\boldsymbol{\eta}}_1} - \boldsymbol{J}_{\tilde{\boldsymbol{\eta}}_1\tilde{\boldsymbol{\eta}}_2}\boldsymbol{J}_{\tilde{\boldsymbol{\eta}}_2\tilde{\boldsymbol{\eta}}_2}^{-1}\boldsymbol{J}_{\tilde{\boldsymbol{\eta}}_1\tilde{\boldsymbol{\eta}}_2}^{\mathrm{T}}, \tag{11}$$

where $\boldsymbol{J}_{\tilde{\boldsymbol{\eta}}_1\tilde{\boldsymbol{\eta}}_1}$, $\boldsymbol{J}_{\tilde{\boldsymbol{\eta}}_1\tilde{\boldsymbol{\eta}}_2}$, and $\boldsymbol{J}_{\tilde{\boldsymbol{\eta}}_2\tilde{\boldsymbol{\eta}}_2}$ are obtained from the channel FIM $\boldsymbol{J}_{\tilde{\boldsymbol{\eta}}}$ in (10) as outlined by (8).

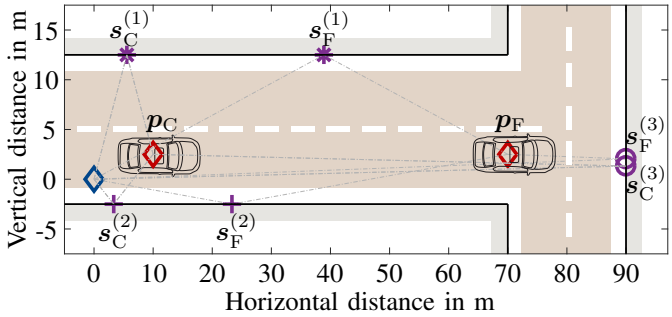

Fig. 2. Geometric constellations considered during the numerical analysis.

D. From Channel Parameters to Position-related Parameters

The EFIM in (11) can be studied via the information inequality in (6) to obtain insights regarding the channel estimation capabilities. Recall, though, that our main goal is to investigate the feasibility of joint positioning, orientation estimation, synchronization, and mapping. In the pursuit of obtaining the FIM $\boldsymbol{J}_{\boldsymbol{\eta}}$ of these position-related parameters, we apply a Jacobian transformation $\boldsymbol{T}$ to the EFIM in (11). This transformation can be directly derived from the geometric relationships between channel parameters and position-related parameters shown in (5). Particularly, the transformation matrix $\boldsymbol{T}$ is given by $\boldsymbol{T} = \partial\tilde{\boldsymbol{\eta}}_1/\partial\boldsymbol{\eta}$. All non-zero entries of $\boldsymbol{T}$ are summarized in Appendix B. Finally, we obtain the FIM[3] $\boldsymbol{J}_{\boldsymbol{\eta}}$ of the position-related parameters via

$$\boldsymbol{J}_{\boldsymbol{\eta}} = \boldsymbol{T}\boldsymbol{J}^{\mathrm{e}}_{\tilde{\boldsymbol{\eta}}_1}\boldsymbol{T}^{\mathrm{T}}. \tag{12}$$

E. Cramér-Rao Lower Bound

Before advancing to the numerical analysis in the next section, we define the position error bound (PEB), orientation error bound (OEB), synchronization error bound (SEB), and mapping error bound (MEB) based on the FIM in (12).

$$\mathrm{PEB} = \sqrt{\mathrm{tr}\left(\boldsymbol{J}_{\boldsymbol{\eta}}^{-1}(\boldsymbol{e}_1\boldsymbol{e}_1^{\mathrm{T}} + \boldsymbol{e}_2\boldsymbol{e}_2^{\mathrm{T}})\right)}, \tag{13a}$$

$$\mathrm{OEB} = \sqrt{\boldsymbol{e}_3^{\mathrm{T}}\boldsymbol{J}_{\boldsymbol{\eta}}^{-1}\boldsymbol{e}_3}, \tag{13b}$$

$$\mathrm{SEB} = c\sqrt{\boldsymbol{e}_4^{\mathrm{T}}\boldsymbol{J}_{\boldsymbol{\eta}}^{-1}\boldsymbol{e}_4}, \tag{13c}$$

$$\mathrm{MEB} = \sqrt{\mathrm{tr}\left(\boldsymbol{J}_{\boldsymbol{\eta}}^{-1}(\boldsymbol{e}_5\boldsymbol{e}_5^{\mathrm{T}} + \cdots + \boldsymbol{e}_{(2N_{\mathrm{P}}+4)}\boldsymbol{e}_{(2N_{\mathrm{P}}+4)}^{\mathrm{T}})\right)}, \tag{13d}$$

where $\boldsymbol{e}_i$ is the ith Euclidean basis vector of length $2N_{\mathrm{P}} + 4$.

IV. Numerical Evaluation

A. Simulation Parameters

We consider the geometric constellations depicted in Fig. 2 which show an urban corner with reflecting walls illustrated by solid black lines. Blue and red diamonds depict the positions of the base station and UE that are both equipped with uniform linear arrays (ULAs) whose orientations are $\phi = \alpha = 0$. Both arrays consist of $N_{\mathrm{TX}} = N_{\mathrm{RX}} = 20$ antennas. Two UE positions are considered: $\boldsymbol{p}_{\mathrm{C}} = [10\ 2.5]^{\mathrm{T}}$m and $\boldsymbol{p}_{\mathrm{F}} = [70\ 2.5]^{\mathrm{T}}$m. The corresponding specular reflection points are indicated by magenta asterisks, pluses, and circles. During the analyses in the sections IV-B and IV-C, only $\boldsymbol{p}_{\mathrm{F}}$ and $\boldsymbol{s}_{\mathrm{F}}^{(1)}$ are considered.

We consider $N_{\mathrm{SC}} = 256$ subcarriers with $\Delta f = 240$ KHz modulated on a carrier with $f_{\mathrm{C}} = 28$ GHz. Pilot symbols are randomly chosen from a quadrature phase shift keying (QPSK) alphabet and precoding vectors are chosen such that $\boldsymbol{f}_j = \boldsymbol{a}_{\mathrm{TX}}(\theta_{\mathrm{TX}}^{(j)} + n_{\theta,\mathrm{f}}), j \in \{0, 1\}$, where $\mathsf{n}_{\theta,\mathrm{f}} \sim \mathcal{N}(0, \sigma_{\theta,\mathrm{f}}^2)$ is a zero-mean Gaussian angular offset with standard deviation $\sigma_{\theta,f} = 10°/N_{\mathrm{TX}}$. The random variable $\mathsf{n}_{\theta,\mathrm{f}}$ models the estimation error of the AODs at the transmitter in a simplistic way. The noise power spectral density is $N_0 = kT_{\mathrm{sys}}$ with $T_{\mathrm{sys}} = 300$ K and k denotes the Boltzmann constant. Path loss coefficients $\gamma^{(j)}, \forall j$ are computed according to the free space loss equation and reflection loss is $\rho^{(1)} = 2$ unless stated differently. All results are averaged over $N_{\mathrm{MC}} = 1000$ Monte Carlo realizations.

B. Parameter Scaling

Here, we scale relevant system parameters by factor κ to observe their effects on the performance bounds in (13). We choose E_{S} such that the SNR at $\kappa = 1$ is $\mathrm{SNR} = 0$ dB. Figure 3 depicts the impact of scaling on the error bounds. We can observe that increasing the number N_{TX} of transmit antennas improves all error bounds and provides the most profound reductions of the bounds. Scaling the bandwidth via the subcarrier spacing Δf improves the PEB, SEB, and MEB. For large κ, the reduction due to an increase in bandwidth is negated by the increased noise power incurred by larger bandwidth and hence the curves saturate. Increasing the bandwidth by scaling the number N_{SC} of subcarriers degrades the PEB, SEB, and MEB because the bandwidth per carrier remains constant but the SNR decreases (more noise is accumulated over the carriers while E_{s} is constant). Bear in mind that, for fair comparison, we chose constant E_{s} rather than constant transmit power. Observe that all position-related parameters can be estimated accurately already for small values of κ.

C. Reflection Loss

The impact of the reflection loss is studied in the case of known and unknown clock offset ϵ. We consider the parameters introduced in IV-A and E_{S} is again chosen such that the SNR at $\rho^{(1)} = 1$ is $\mathrm{SNR} = 0$ dB. The results depicted in Fig. 4 show the relative increase of the bounds with respect to the value at $\rho^{(1)} = 1$, e.g. $\Delta\mathrm{PEB} = (\mathrm{PEB}(\rho^{(1)}) - \mathrm{PEB}(\rho^{(1)} = 1))/\mathrm{PEB}(\rho^{(1)} = 1)$. We can observe that the OEB is not affected since the orientation is predominantly resolved via the AOD and AOA of the LOS path. However, if ϵ is unknown, the PEB, SEB, and MEB increase rapidly as the attenuation of the NLOS path increases. The main problem is that the channel parameters of the NLOS path cannot be estimated accurately if SNR on that path is low. Hence the clock offset cannot be resolved well, making also positioning and mapping imprecise. It is worth noting that providing high-accuracy situational awareness becomes quickly infeasible as the reflection loss increases if ϵ is unknown. Practical values of the reflection loss depend strongly on the material, carrier frequency, etc. Reported values [16] at $f_{\mathrm{c}} = 28$ GHz range from $\rho_{\mathrm{dB}}^{(1)} \approx 4$ dB

[3]Note that the FIM $\boldsymbol{J}_{\boldsymbol{\eta}}$ of the position-related parameters is determined based on the EFIM $\boldsymbol{J}^{\mathrm{e}}_{\tilde{\boldsymbol{\eta}}_1}$ of the channel parameters and hence can be seen as an EFIM rather than an FIM. For simplicity and with a slight abuse of the notation, we call $\boldsymbol{J}_{\boldsymbol{\eta}}$ an FIM.

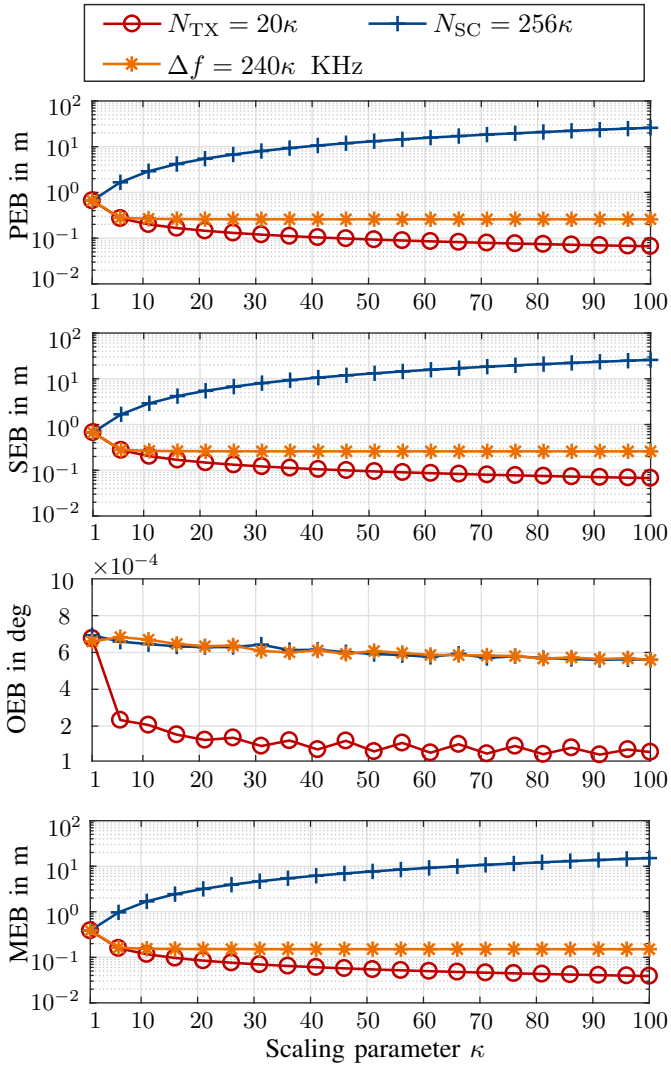

Fig. 3. PEB, SEB, OEB, and MEB versus scaling of system parameters.

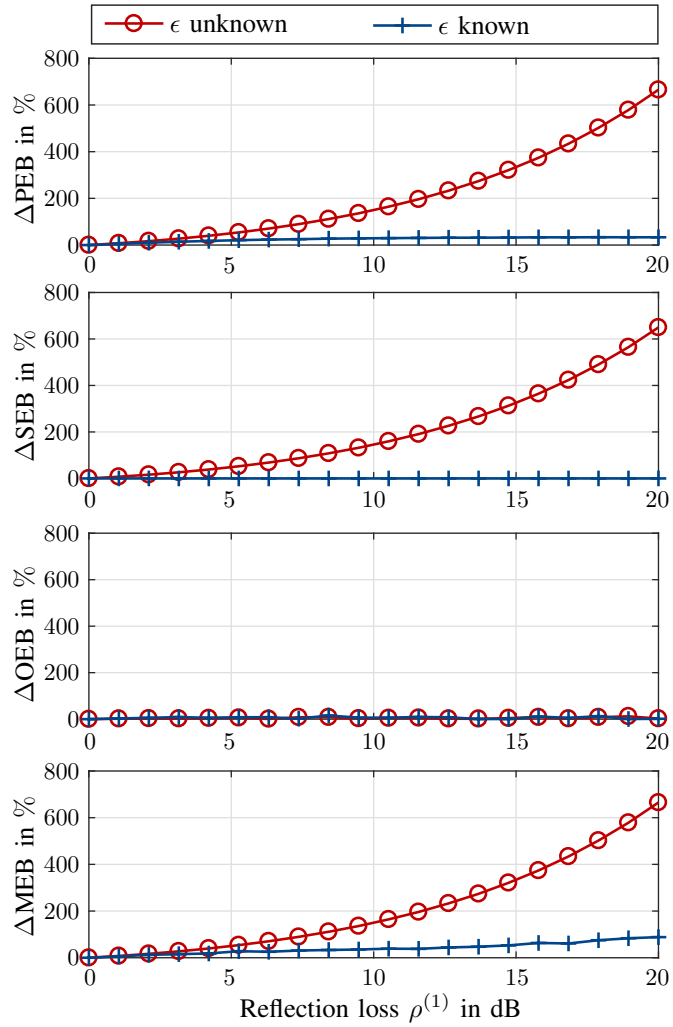

Fig. 4. Relative increase ΔPEB, ΔSEB, ΔOEB, and ΔMEB of the error bounds versus increasing reflection loss $\rho^{(1)}$.

(glass) over $\rho^{(1)}_{\mathrm{dB}} \approx 8$ dB (concrete and tiles) to $\rho^{(1)}_{\mathrm{dB}} \approx 18$ dB (wood).

D. Geometry

We investigate the impact of the geometry on the PEB (SEB, OEB, and MEB are omitted due to space constraints) in Fig. 5 and consider the parameters introduced in IV-A. The geometric constellations are depicted in Fig. 2. Every marker corresponds to one geometric constellation and the corresponding E_{S} are chosen such that $\mathrm{SNR}=0$ dB (identical SNRs). Observe that, in addition to our previous findings, the geometry of the scenario is also key and certain UE-reflector-base-station constellations provide poor estimation accuracy by nature. It is worth noting, however, that in a non-static tracking application [2], channel measurements from different geometric constellations can be fused which can enable accurate situational awareness also in scenarios with poor geometry.

V. Conclusions

We investigated the feasibility of situational awareness in millimeter wave massive multiple-input multiple-output systems. Particularly, we employed the concept of Fisher information and the Cramér-Rao lower bound to show that the achievable accuracy of position, orientation, clock offset, and map estimation can be greatly improved by increasing the number of antennas. Moreover, our results highlight that increasing the number of antennas by a constant factor provides higher gains in terms of accuracy than increasing the bandwidth by the same factor. Finally, we emphasize that high attenuation on non-line-of-sight paths due to reflection losses degrade the estimation accuracy significantly which can render joint positioning, synchronization, mapping infeasible.

Appendix A
Partial Derivatives of the Noise-free Observation

The partial derivatives $\partial \boldsymbol{\mu}_n^{\mathrm{H}} / \partial [\tilde{\boldsymbol{\eta}}]_l$ of the noise-free observations on subcarrier n are given as:

$$\frac{\partial \boldsymbol{\mu}_n^{\mathrm{H}}}{\partial \tau^{(j)}} = \left(\frac{\partial}{\partial \tau^{(j)}} \xi_n^{(j)*} \right) \tilde{\boldsymbol{x}}_n^{\mathrm{H}} \boldsymbol{F}^{\mathrm{H}} \boldsymbol{a}_{\mathrm{TX}}(\theta_{\mathrm{TX}}^{(j)}) \boldsymbol{a}_{\mathrm{RX}}^{\mathrm{H}}(\theta_{\mathrm{RX}}^{(j)}), \quad (14a)$$

$$\frac{\partial \boldsymbol{\mu}_n^{\mathrm{H}}}{\partial \theta_{\mathrm{TX}}^{(j)}} = \xi_n^{(j)*} \tilde{\boldsymbol{x}}_n^{\mathrm{H}} \boldsymbol{F}^{\mathrm{H}} \left(\frac{\partial}{\partial \theta_{\mathrm{TX}}^{(j)}} \boldsymbol{a}_{\mathrm{TX}}(\theta_{\mathrm{TX}}^{(j)}) \right) \boldsymbol{a}_{\mathrm{RX}}^{\mathrm{H}}(\theta_{\mathrm{RX}}^{(j)}), \quad (14b)$$

$$\frac{\partial \boldsymbol{\mu}_n^{\mathrm{H}}}{\partial \theta_{\mathrm{RX}}^{(j)}} = \xi_n^{(j)*} \tilde{\boldsymbol{x}}_n^{\mathrm{H}} \boldsymbol{F}^{\mathrm{H}} \boldsymbol{a}_{\mathrm{TX}}(\theta_{\mathrm{TX}}^{(j)}) \left(\frac{\partial}{\partial \theta_{\mathrm{RX}}^{(j)}} \boldsymbol{a}_{\mathrm{RX}}^{\mathrm{H}}(\theta_{\mathrm{RX}}^{(j)}) \right), \quad (14c)$$

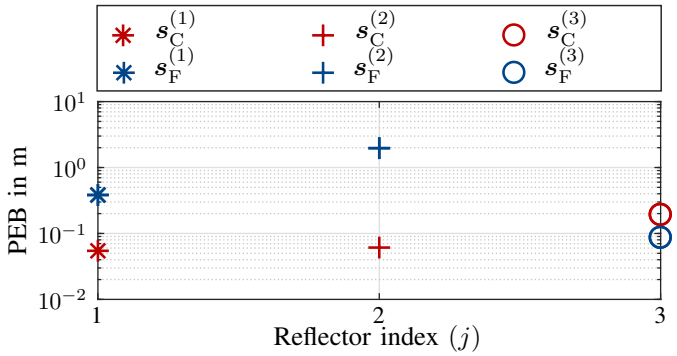

Fig. 5. PEB in different geometric constellations.

$$\frac{\partial \boldsymbol{\mu}_n^{\mathrm{H}}}{\partial h_{\mathrm{I}}^{(j)}} = \left(\frac{\partial}{\partial h_{\mathrm{I}}^{(j)}} \xi_n^{(j)*}\right) \tilde{\boldsymbol{x}}_n^{\mathrm{H}} \boldsymbol{F}^{\mathrm{H}} \boldsymbol{a}_{\mathrm{TX}}(\theta_{\mathrm{TX}}^{(j)}) \boldsymbol{a}_{\mathrm{RX}}^{\mathrm{H}}(\theta_{\mathrm{RX}}^{(j)}), \quad (14d)$$

$$\frac{\partial \boldsymbol{\mu}_n^{\mathrm{H}}}{\partial h_{\mathrm{Q}}^{(j)}} = \left(\frac{\partial}{\partial h_{\mathrm{Q}}^{(j)}} \xi_n^{(j)*}\right) \tilde{\boldsymbol{x}}_n^{\mathrm{H}} \boldsymbol{F}^{\mathrm{H}} \boldsymbol{a}_{\mathrm{TX}}(\theta_{\mathrm{TX}}^{(j)}) \boldsymbol{a}_{\mathrm{RX}}^{\mathrm{H}}(\theta_{\mathrm{RX}}^{(j)}). \quad (14e)$$

The remaining partial derivatives in (14) are readily shown to be

$$\frac{\partial \xi_n^{(j)*}}{\partial \tau^{(j)}} = i \frac{2\pi n}{N_{\mathrm{SC}} T_{\mathrm{S}}} \xi_n^{(j)*} \quad (15a)$$

$$\frac{\partial \boldsymbol{a}_{\mathrm{TX}}(\theta_{\mathrm{TX}}^{(j)})}{\partial \theta_{\mathrm{TX}}^{(j)}} = -i \Delta_{\mathrm{TX}} \bar{\boldsymbol{k}}(\theta_{\mathrm{TX}}^{(j)}) \boldsymbol{a}_{\mathrm{TX}}(\theta_{\mathrm{TX}}^{(j)}) \quad (15b)$$

$$\frac{\partial \boldsymbol{a}_{\mathrm{RX}}^{\mathrm{H}}(\theta_{\mathrm{RX}}^{(j)})}{\partial \theta_{\mathrm{RX}}^{(j)}} = i \Delta_{\mathrm{RX}} \bar{\boldsymbol{k}}(\theta_{\mathrm{RX}}^{(j)}) \boldsymbol{a}_{\mathrm{RX}}(\theta_{\mathrm{RX}}^{(j)}) \quad (15c)$$

$$\frac{\partial \xi_n^{(j)*}}{\partial h_{\mathrm{I}}^{(j)}} = \frac{\xi_n^{(j)*}}{h^{(j)*}} \quad (15d)$$

$$\frac{\partial \xi_n^{(j)*}}{\partial h_{\mathrm{Q}}^{(j)}} = -i \frac{\xi_n^{(j)*}}{h^{(j)*}} \quad (15e)$$

where $\bar{\boldsymbol{k}}(\theta_{\mathrm{TX}}) \triangleq 2\pi/\lambda[-\sin(\theta_{\mathrm{TX}}) \ \cos(\theta_{\mathrm{TX}})]^{\mathrm{T}}$.

Appendix B
Partial Derivatives of the Transformation

The non-zero partial derivatives of the channel parameters summarized in the following. Those of delays are given by

$$\frac{\partial \tau^{(0)}}{\partial \boldsymbol{p}} = \frac{\boldsymbol{p} - \boldsymbol{q}}{c \left\| \boldsymbol{p} - \boldsymbol{q} \right\|}, \quad (16a)$$

$$\frac{\partial \tau^{(j)}}{\partial \boldsymbol{p}} = \frac{\boldsymbol{p} - \boldsymbol{s}^{(j)}}{c \left\| \boldsymbol{p} - \boldsymbol{s}^{(j)} \right\|}, \quad j > 0, \quad (16b)$$

$$\frac{\partial \tau^{(j)}}{\partial \boldsymbol{s}^{(j)}} = \frac{\boldsymbol{s}^{(j)} - \boldsymbol{q}}{c \left\| \boldsymbol{q} - \boldsymbol{s}^{(j)} \right\|} + \frac{\boldsymbol{s}^{(j)} - \boldsymbol{p}}{c \left\| \boldsymbol{p} - \boldsymbol{s}^{(j)} \right\|}, \quad j > 0, \quad (16c)$$

$$\frac{\partial \tau^{(j)}}{\partial \epsilon} = 1, \quad \forall j, \quad (16d)$$

where c is the speed of light. The corresponding partial derivatives of AODs and AOAs are given by

$$\frac{\partial \theta_{\mathrm{TX}}^{(0)}}{\partial \boldsymbol{p}} = \frac{\left(-\boldsymbol{e}_1 \boldsymbol{e}_2^{\mathrm{T}} + \boldsymbol{e}_2 \boldsymbol{e}_1^{\mathrm{T}}\right)(\boldsymbol{p} - \boldsymbol{q})}{\left\| \boldsymbol{p} - \boldsymbol{q} \right\|^2}, \quad (17a)$$

$$\frac{\partial \theta_{\mathrm{TX}}^{(j)}}{\partial \boldsymbol{s}^{(j)}} = \frac{\left(-\boldsymbol{e}_1 \boldsymbol{e}_2^{\mathrm{T}} + \boldsymbol{e}_2 \boldsymbol{e}_1^{\mathrm{T}}\right)(\boldsymbol{s}^{(j)} - \boldsymbol{q})}{\left\| \boldsymbol{s}^{(j)} - \boldsymbol{q} \right\|^2}, j > 0 \quad (17b)$$

and

$$\frac{\partial \theta_{\mathrm{RX}}^{(0)}}{\partial \boldsymbol{p}} = \frac{\partial \theta_{\mathrm{TX}}^{(0)}}{\partial \boldsymbol{p}}, \quad (18a)$$

$$\frac{\partial \theta_{\mathrm{RX}}^{(j)}}{\partial \boldsymbol{p}} = \frac{\left(-\boldsymbol{e}_1 \boldsymbol{e}_2^{\mathrm{T}} + \boldsymbol{e}_2 \boldsymbol{e}_1^{\mathrm{T}}\right)(\boldsymbol{p} - \boldsymbol{s}^{(j)})}{\left\| \boldsymbol{p} - \boldsymbol{s}^{(j)} \right\|^2}, j > 0 \quad (18b)$$

$$\frac{\partial \theta_{\mathrm{RX}}^{(j)}}{\partial \boldsymbol{s}^{(j)}} = -\frac{\partial \theta_{\mathrm{RX}}^{(j)}}{\partial \boldsymbol{p}}, j > 0 \quad (18c)$$

$$\frac{\partial \theta_{\mathrm{RX}}^{(j)}}{\partial \alpha} = -1, \forall j. \quad (18d)$$

References

[1] 3rd Generation Partnership Project (3GPP), "TR 21.915," Tech. Rep. V15.0.0, October 2019.

[2] R. Mendrzik, F. Meyer, G. Bauch, and M. Z. Win, "Enabling situational awareness in millimeter wave massive MIMO systems," *IEEE J. Sel. Topics Signal Process.*, vol. 13, no. 5, pp. 1196–1211, Sep. 2019.

[3] H. Wymeersch, N. Garcia, H. Kim, G. Seco-Granados, S. Kim, F. Wen, and M. Fröhle, "5G mmWave downlink vehicular positioning," in *Proc. IEEE GLOBECOM-18*, Dec. 2018.

[4] R. Mendrzik, F. Meyer, G. Bauch, and M. Win, "Fast Inference for Situational Awareness in 5G Millimeter Wave Massive MIMO Systems," in *2019 IEEE 20th International Workshop on Signal Processing Advances in Wireless Communications (SPAWC)*, July 2019, pp. 1–5.

[5] A. Kakkavas, M. H. Castañeda García, R. A. Stirling-Gallacher, and J. A. Nossek, "Performance limits of single-anchor millimeter-wave positioning," *IEEE Transactions on Wireless Communications*, vol. 18, no. 11, pp. 5196–5210, Nov. 2019.

[6] M. Ulmschneider, C. Gentner, and A. Dammann, "Data association among physical and virtual radio transmitters with visibility regions," in *2019 IEEE 90th Vehicular Technology Conference (VTC2019-Fall)*, Sep. 2019, pp. 1–7.

[7] R. D. Taranto, S. Muppirisetty, R. Raulefs, D. T. Slock, T. Svensson, and H. Wymeersch, "Location-aware communications for 5G networks: How location information can improve scalability, latency, and robustness of 5G," *IEEE Signal Process. Mag.*, vol. 31, no. 6, pp. 102–112, Nov. 2014.

[8] A. Guerra, F. Guidi, and D. Dardari, "Single-anchor localization and orientation performance limits using massive arrays: MIMO vs. beamforming," *IEEE Trans. Wireless Commun.*, vol. 17, no. 8, pp. 5241–5255, Aug. 2018.

[9] Z. Abu-Shaban, X. Zhou, T. Abhayapala, G. Seco-Granados, and H. Wymeersch, "Performance of location and orientation estimation in 5G mmWave systems: Uplink vs downlink," in *Proc. IEEE WCNC-18*, Apr. 2018.

[10] R. Mendrzik, H. Wymeersch, G. Bauch, and Z. Abu-Shaban, "Harnessing NLOS components for position and orientation estimation in 5G millimeter wave MIMO," *IEEE Trans. Wireless Commun.*, vol. 18, no. 1, pp. 93–107, Jan 2019.

[11] R.-W. Heath, N. González-Prelcic, S. Rangan, W. Roh, and A.-M. Sayeed, "An overview of signal processing techniques for millimeter wave MIMO systems," *IEEE J. Sel. Topics Signal Process.*, vol. 10, no. 3, pp. 436–453, Apr. 2016.

[12] H. L. V. Trees, *Detection, Estimation, and Modulation Theory: Radar-Sonar Signal Processing and Gaussian Signals in Noise*. Melbourne, FL, USA: Krieger Publishing Co., Inc., 1992.

[13] H. V. Poor, *An Introduction to Signal Detection and Estimation (2Nd Ed.)*. Berlin, Heidelberg: Springer-Verlag, 1994.

[14] I. Reuven and H. Messer, "A Barankin-type lower bound on the estimation error of a hybrid parameter vector," *IEEE Trans. Inf. Theory*, vol. 43, no. 3, pp. 1084–1093, May 1997.

[15] P. Tichavsky, C. H. Muravchik, and A. Nehorai, "Posterior Cramer-Rao bounds for discrete-time nonlinear filtering," *IEEE Trans. Signal Process.*, vol. 46, no. 5, pp. 1386–1396, May 1998.

[16] B. G. Choi, W. H. Jeong, and K. S. Kim, "Characteristics Analysis of Reflection and Transmission According to Building Materials in the Millimeter Wave Band," in *Proc. Recent Advances on Electroscience and Computers*, 2015, pp. 154–158.